International Journal of Radiation Oncology biology • physics

www.redjournal.org

Technological Advances

Measured Neutron Spectra and Dose Equivalents From a Mevion Single-Room, Passively Scattered Proton System Used for Craniospinal Irradiation

Rebecca M. Howell, PhD,* Eric A. Burgett, PhD,† Daniel Isaacs, BS,† Samantha G. Price Hedrick, PhD,‡ Michael P. Reilly, PhD,‡ Leith J. Rankine, MS,‡ Kevin K. Grantham, PhD,‡ Stephanie Perkins, MD,‡ and Eric E. Klein, PhD‡

**Department of Radiation Physics, The University of Texas M. D. Anderson Cancer Center, Houston, Texas; †Department of Nuclear Engineering, Idaho State University, Pocatello, Idaho; and ‡Department of Radiation Oncology, Washington University, St. Louis, Missouri*

Received Oct 6, 2015, and in revised form Nov 19, 2015. Accepted for publication Dec 14, 2015.

Summary

Craniospinal irradiation (CSI) with protons is effective mainly owing to distal dose sparing. A concern is the impact of neutron dose outside of the treatment fields. Measuring neutron dose is challenging because of the need to accurately account for the energy spectrum. This comprehensive measurement study addresses this issue specifically for CSI on the single-room Mevion S250 proton system.

Purpose: To measure, in the setting of typical passively scattered proton craniospinal irradiation (CSI) treatment, the secondary neutron spectra, and use these spectra to calculate dose equivalents for both internal and external neutrons delivered via a Mevion single-room compact proton system.

Methods and Materials: Secondary neutron spectra were measured using extended-range Bonner spheres for whole brain, upper spine, and lower spine proton fields. The detector used can discriminate neutrons over the entire range of the energy spectrum encountered in proton therapy. To separately assess internally and externally generated neutrons, each of the fields was delivered with and without a phantom. Average neutron energy, total neutron fluence, and ambient dose equivalent [H*(10)] were calculated for each spectrum. Neutron dose equivalents as a function of depth were estimated by applying published neutron depth−dose data to in-air H*(10) values.

Results: For CSI fields, neutron spectra were similar, with a high-energy direct neutron peak, an evaporation peak, a thermal peak, and an intermediate continuum between the evaporation and thermal peaks. Neutrons in the evaporation peak made the largest contribution to dose equivalent. Internal neutrons had a very low to negligible

Reprint requests to: Rebecca M. Howell, PhD, Department of Radiation Physics, The University of Texas M. D. Anderson Cancer Center, Houston, TX 77030. Tel: (713) 745-8999; E-mail: rhowell@mdanderson.org

Conflict of interest: none.

Supplementary material for this article can be found at www.redjournal.org.

Acknowledgments—The authors thank Brad Hawkins, Jeff Heine, Caesar Chiaradonna, and Alan Anganes, the Mevion engineers who participated in more than 40 hours of measurements, particularly for their expertise in operating the machine at very low dose rates, thereby making possible the use of an active detection technique. The authors also thank Ms. Kathryn Hale from The University of Texas M. D. Anderson Cancer Center Department of Scientific Publications for assistance in editing the manuscript; and Dr Phillip J. Taddei for his feedback on a draft of the manuscript.

Int J Radiation Oncol Biol Phys, Vol. 95, No. 1, pp. 249–257, 2016

http://dx.doi.org/10.1016/j.ijrobp.2015.12.356

The resulting dose equivalent was found to be in line with other proton systems.

contribution to dose equivalent compared with external neutrons, largely attributed to the measurement location being far outside the primary proton beam. Average energies ranged from 8.6 to 14.5 MeV, whereas fluences ranged from 6.91×10^6 to 1.04×10^7 n/cm^2/Gy, and H* (10) ranged from 2.27 to 3.92 mSv/Gy.

Conclusions: For CSI treatments delivered with a Mevion single-gantry proton therapy system, we found measured neutron dose was consistent with dose equivalents reported for CSI with other proton beamlines.

Introduction

Craniospinal irradiation (CSI), which involves irradiating the entire craniospinal axis, is part of the standard of care in the treatment of several pediatric brain tumors, including medulloblastoma, the second most common solid tumor in children (1-3). Proton radiation therapy substantially reduces radiation dose to organs situated outside the craniospinal axis (4-9) compared with photon therapy because of its lower entrance dose and essentially no exit dose. Despite these proven advantages, secondary neutrons, an unavoidable consequence of any proton therapy technique, remain a concern. This concern is somewhat heightened for passively scattered versus magnetically scanned techniques because of the additional high atomic number materials in the beamline for the former (10, 11). Dose from secondary neutrons is of particular concern in proton CSI because this treatment is almost universally utilized for children and adolescents, who often survive many decades after diagnosis (12-14) and are at significant risk of radiation-related late effects, including second malignancies in the years following their treatment (15, 16).

Compared with therapeutic protons, secondary neutron exposure is low. Nonetheless, it is important to understand its contribution to the overall patient dose. Doses from neutrons generated external to the patient (external neutrons) are highly dependent on the proton beam incident on the patient, which depends on the design of the proton therapy machine itself and treatment-specific devices within the beamline (17). Doses from neutrons generated within the patient (internal neutrons) increase with beam range and treatment volume irradiated (ie, field size) (18, 19).

Doses from both internal and external neutrons calculated by Monte Carlo simulations of passively scattered proton CSI have been reported in the literature (19-23), but data based on spectra measurements are lacking. This gap in the literature is a direct consequence of the limitations of various neutron detectors, including limited energy discrimination, limited response to neutrons having energies greater than 20 MeV, and pulse pile-up for active detectors (Kry et al, unpublished). Extended-range Bonner spheres with appropriate energy sensitivity have been used in 2 other studies (24, 25) to measure secondary neutron spectra from proton therapy, but neither study considered CSI fields, which tend to have apertures with substantial exposed brass. Those studies were carried out specifically for the Hitachi (Hitachi Probeat; Hitachi America Limited, Tarrytown, NJ) and IBA (Ion Beam Applications SA, Louvain-la-Neuve, Belgium) beamlines. Furthermore, the extensive Monte Carlo data for neutron doses from proton CSI that have been reported are mainly for Hitachi proton beam lines, with a lack of neutron doses reported for other systems now in use. The Mevion (Mevion s250; Mevion Medical Systems, Littleton, MA) single-room compact proton systems are particularly noteworthy because worldwide 4 units are currently clinically operational, 2 are under installation (accelerator in place), and 2 more are under construction (at the time of this submission) (26).

The objectives of this study were, for a passively scattered proton CSI treatment delivered via a single-room compact proton system, (*1*) to measure the secondary neutron spectra with a detector that can discriminate neutrons over the entire range of the energy spectra encountered in proton therapy; (*2*) to use the measured neutron spectra to calculate dose equivalents; and (*3*) to report these data for both internal and external neutrons specifically.

Methods and Materials

Measurements

Measurements were made in a single-room passively scattered proton therapy treatment room, which houses a synchrocyclotron accelerator system (Mevion 250, Mevion Medical Systems). This system can deliver passively scattered proton beams up to 250 MeV utilizing a 9.6-Tesla superconducting magnet, which handles up to 2000 amps of current. The passive scattering system includes an initial scatterer, range modulator wheels, secondary scatterers, and various absorbers to give range designation and flat profiles. The range and modulation are defined as the distance in centimeters from the surface to the distal 90% dose and from the proximal 95% dose to the distal 90% dose, respectively. The field size is defined with either a large (25-cm diameter) or small (14-cm diameter) applicator.

Table 1 Summary of the beam delivery parameters for each craniospinal irradiation field for which neutrons were measured

Field type	Beam incident on	Gantry angle (°)	Couch angle (°)	Aperture size	Blocked by aperture (%)	Range (cm)	Modulation (cm)
Whole brain	Air, water, anthropomorphic	90	270	Large	51.5	17	16
Upper spine	Air, water	0	270	Large	57.5	10	8
Lower spine	Air, water, plastic water	0	270	Large	61.2	10	8

All measurements were performed at a distance of 50 cm (along the patient axis) from isocenter to ensure that our active detector was not affected by pulse pile-up. The beam delivery parameters are summarized in Table 1, and the treatment fields comprised whole brain, upper spine, and lower spine based on an actual patient's treatment. Each treatment field was delivered using the large aperture (nominal open diameter of 25 cm at 2 m physical source-to-axis distance), into which treatment field−specific apertures were added; percentage of blocking is listed in Table 1. To separately assess internally and externally generated neutrons, each of the 3 treatments was repeated with and without a water phantom ($35 \times 35 \times 35$ cm^3) directly under the beam at isocenter. Additionally, the whole-brain treatment was delivered to an anthropomorphic phantom (head to clavicle) at isocenter to evaluate whether internal neutron production differed for water and for a phantom having a more complex elemental composition. Finally, to assess whether there was any difference in internal neutrons generated in water and those generated in plastic water, the lower spine field was also delivered with plastic water at isocenter. The experimental setups for the brain and upper spine irradiations are shown in Figure 1 in the Supplementary Material (available online at www.redjournal.org).

For each of the clinical field types, we performed proton dose measurements in a water phantom to determine the exact therapeutic proton dose delivered in grays (Gy) per monitor unit (MU). These data were then used to normalize the measured neutron data per proton Gy. Because measurements were performed with dose rates that are below those used clinically, dose rate linearity was tested from clinical rates (120 to 200 MU/min) down to those used in this study (15 to 20 MU/min).

Neutron detection equipment

We used an extended-range Bonner sphere spectrometer, the Bonner sphere extension (BSE) measurement system, to perform measurements. The advantage of this detection system is that, unlike standard Bonner spheres, it is sensitive to neutrons over the entire energy range encountered in proton therapy (thermal to 250 MeV) and has sufficient energy discrimination for spectral measurements. We briefly summarize the detection system here; a more thorough description is available in the literature (25, 27, 28). The BSE is a modular multisphere system with a total of 18 sphere combinations that includes 6 standard polyethylene Bonner spheres (ranging from 5.1 cm to 30.5 cm diameters) and 12 extended-sphere combinations. The extended spheres include various combinations that have either a 7.6-cm or a 12.7-cm Bonner sphere surrounded by a copper, tungsten, or lead shell that can be further encased in an outer polyethylene sphere. In the present study we used an active ^{6}LiI(Eu) scintillator (Ludlum Measurements, Sweetwater, TX), necessitating accelerator engineers to tune the beam to very low proton dose rates to avoid pulse pile-up and erroneous results. Using the active detector, we were able to measure sufficient neutron counts to achieve uncertainties of $<1\%$ with very short beam-on times, on average 1 to 1.5 minutes. In total we carried out 8 sets of measurements for various CSI fields (described in the following section), each set including 18 separate measurements with the detector centered inside each of the 18 detector-sphere combinations. These data required mathematical deconvolution to determine the neutron spectra.

Spectrum unfolding

Data for each of the 8 sets of measurements were unfolded by using the MAXimum Entropy Deconvoloution (MAXED MXD_FC33) algorithm, of the UMG software package, version 3.3.44 (29, 30). Spectrum unfolding required measured data, an a priori (ie, starting) spectrum, and response functions for each detector sphere combination. A starting spectrum was determined by using a previously described Bayesian statistical method (25, 29). A separate response function was previously calculated (27, 28) for the BSE detector-sphere combinations using the Monte Carlo N-Particle Code eXtended (MCNPX) code (31).

Calculated neutron parameters

The average neutron energy and total neutron fluence were calculated for each measured neutron spectrum over the entire energy range from thermal up to the maximum neutron energy. Because neutrons with energy less than 10 keV have a negligible contribution to the dose equivalent, fluence and average energy were also computed without these low-energy neutrons. Ambient dose equivalents [H* (10)] were calculated by applying International Commission on Radiation Protection and Measurements publication 74 conversion coefficients (32, 33) to the fluence spectra.

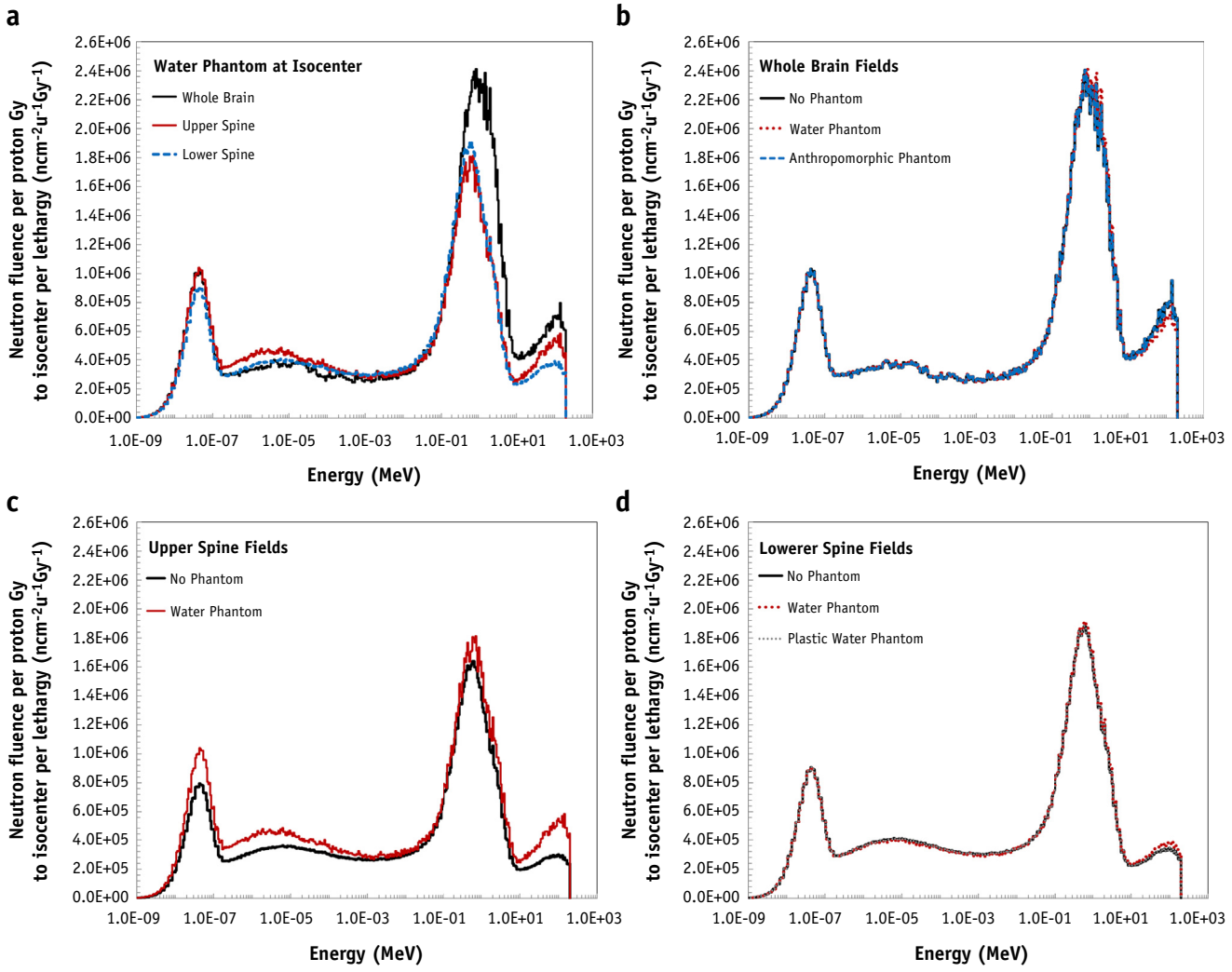

Fig. 1. Comparison of neutron fluence spectra measured at a distance of 50 cm from isocenter for passively scattered proton craniospinal irradiation fields delivered to (a) whole brain, upper spine, and lower spine fields incident on a $35 \times 35 \times 35$-cm^3 water phantom at the isocenter, (b) whole-brain fields, (c) upper spine fields, and (d) lower spine fields. Data in (b), (c), and (d) were measured with no phantom and water phantom at isocenter. For (b) and (d), additional measurements were performed with anthropomorphic and plastic water phantoms at isocenter, respectively.

In a clinical CSI treatment, many organs of interest are much closer to the proton fields than our measurement location of 50 cm from the field isocenter. Thus, H* (10) values at 30 cm from isocenter were approximated by applying an analytical function relating dose and distance from the isocenter to the measured H* (10) data at 50 cm. The analytical function was derived from a series of spectra measurements that were performed using the small aperture with a solid brass insert added to achieve a "closed field." This beamline configuration made it possible to place the detector closer to the isocenter without any pulse pile-up because the neutron fluence for the small aperture field was substantially (approximately 2-fold) lower than for CSI fields that required the large aperture. With this configuration, we performed in-air spectra measurements with the BSE measurement system at isocenter and at 40 cm and 100 cm from the isocenter. The H* (10) at each location were computed and plotted as function of distance from isocenter (x). The data were fit to a second order polynomial model; dose $= 0.0003x^2 - 0.0598x + 3.85$ ($R^2 = 0.98$). Using these data, we calculated a ratio of 1.44 for neutron doses at 30 cm compared with 50 cm from isocenter.

Neutron dose falls off rapidly with depth in a patient (Kry et al, unpublished). Thus, H* (10), an in-air quantity, will overestimate patient dose. As such, to provide realistic estimates of dose in a patient, we estimated neutron dose equivalent as a function of depth by applying published neutron depth–dose data (34) to the in-air H* (10) values. This methodology has been previously reported in the literature (35-37) and is also recommended in an upcoming Task Group Report from the American Association of Physicists in Medicine (Kry et al, unpublished). Depth–dose curves were selected on the basis of the

average neutron energies at 30 cm (13.5 MeV) and 50 cm (11.7 MeV) from isocenter. Finally, we multiplied neutron dose equivalent per therapeutic Gy by 23.4 to estimate the values for a full course of CSI for low- to mid-grade medulloblastoma. However, because our estimated dose equivalents at depth were not specific to any organs, we could not apply organ weighting factors, and therefore it is not possible to calculate a whole-body effective dose.

Results

The measured neutron spectral fluence for each field type and measurement setup are shown in Figure 1. The differences in treatment type are highlighted in Figure 1a, and the effects of having no phantom versus water, plastic water, or anthropomorphic phantoms are illustrated in Figure 1b–d. The corresponding ambient dose equivalent spectra are shown in Figure 2. Both figures are plotted on a log-linear scale, and fluence and dose equivalent are given per unit lethargy, so that the relative fluence and dose equivalent and contributions from each energy bin are proportional to the area under the histogram.

The average energies, total fluence, and ambient dose equivalents per proton Gy are listed in Table 2 over the energy ranges of thermal to 210 MeV and 10 keV to 210 MeV. When all neutrons are considered, average energies and fluences range from 5.3 MeV to 10.0 MeV and from 1.12×10^7 to 1.52×10^7 n/cm^2/Gy, respectively. When only neutrons greater than 10 keV are considered, average energies are higher, ranging between 8.6 to 14.5 MeV, whereas fluences are lower, ranging from 6.91×10^6 to 1.04×10^7 n/cm^2/Gy. The exclusion of neutrons with energy less than 10 keV made almost no

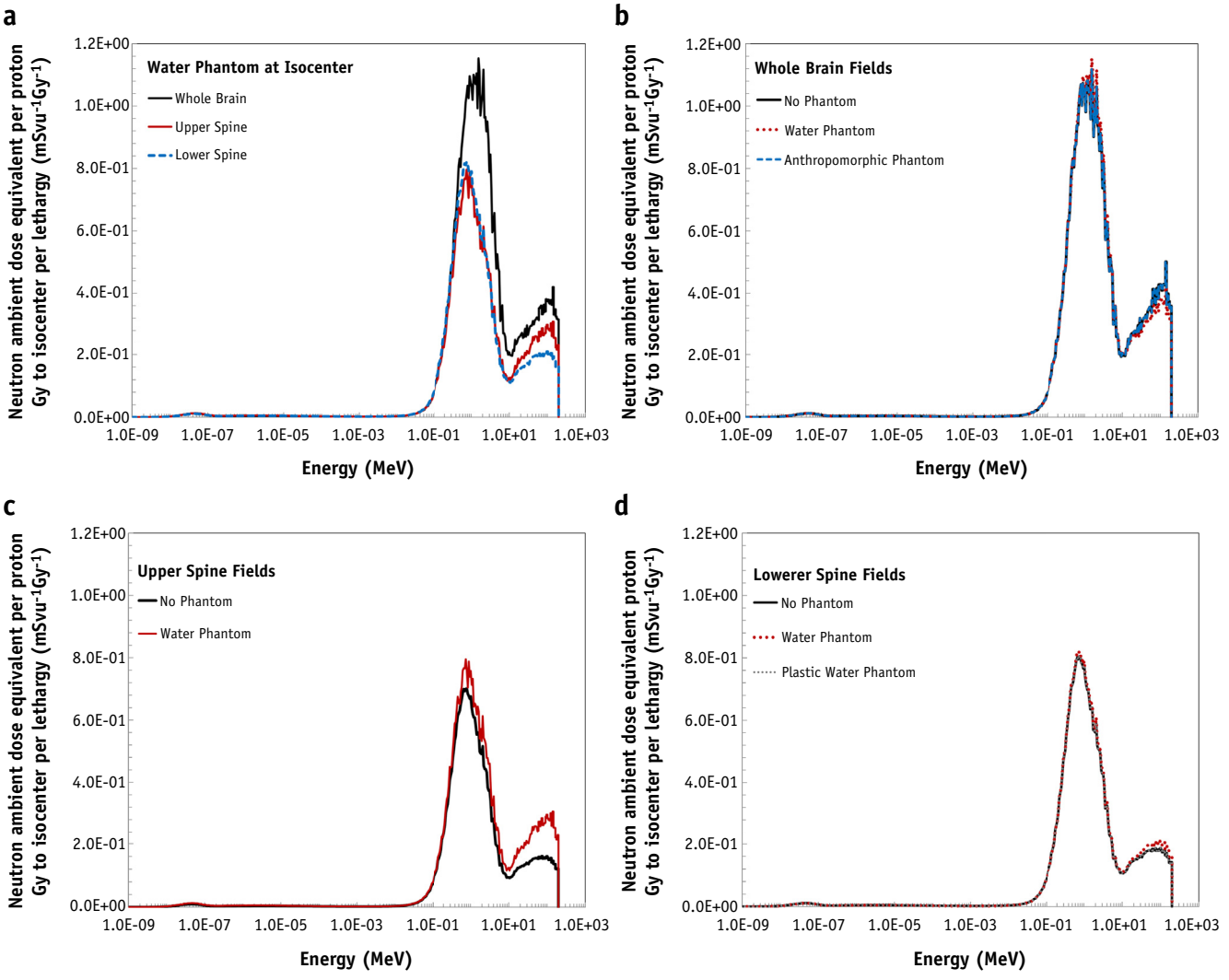

Fig. 2. Comparison of neutron ambient dose equivalent H* (10) spectra measured at a distance of 50 cm from isocenter for passively scattered proton craniospinal irradiation fields delivered to (a) whole brain, upper spine, and lower spine fields incident on a $35 \times 35 \times 35$ cm^3 water phantom at the isocenter, (b) whole-brain fields, (c) upper spine fields, and (d) lower spine fields. Data in (b), (c), and (d) were measured with no phantom and water phantom at isocenter. For (b) and (d), additional measurements were performed with anthropomorphic and plastic water phantoms at isocenter, respectively.

Table 2 Derived neutron parameters per proton Gy delivered to isocenter for whole brain, upper spine, and lower spine craniospinal irradiation fields for measurements at 50 cm from isocenter

		Average energy (MeV)		Fluence per proton Gy (n/cm^2/Gy)		H* (10) per proton Gy (mSv/Gy)	
Field type	Beam incident on	Thermal to 210 MeV	10 keV to 210 MeV	Thermal to 210 MeV	10 keV to 210 MeV	Thermal to 210 MeV	10 keV to 210 MeV
Whole brain	No phantom (air)	10.0	14.5	1.52E+07	1.04E+07	3.95	3.92
	Water phantom	9.9	13.1	1.52E+07	1.04E+07	3.94	3.90
	Anthropomorphic phantom	10.0	14.5	1.52E+07	1.04E+07	3.95	3.92
Upper spine	No phantom (air)	5.3	8.6	1.12E+07	6.91E+06	2.30	2.27
	Water phantom	7.5	12.6	1.34E+07	7.99E+06	2.79	2.75
Lower spine	No phantom (air)	5.4	8.6	1.28E+07	7.92E+06	2.63	2.60
	Water phantom	5.9	9.4	1.29E+07	8.06E+06	2.71	2.68
	Plastic water phantom	5.4	8.6	1.28E+07	7.92E+06	2.63	2.59

Data are indicated separately for in-air and with various different phantoms positioned at isocenter.

difference in the calculated ambient dose equivalent values, which ranged from 2.27 to 3.95 mSv/Gy. These data are separately listed in Table 2 for all 8 measurement scenarios performed at 50 cm from the isocenter.

The estimated dose equivalents at depth in water are listed in Table 3 for 30 cm and 50 cm from isocenter. The data in Table 3 are for a 23.4-Gy prescribed proton dose. Dose at depth is not shown for the 100-cm location because this distance is beyond locations that would be of interest in a patient.

Discussion

We observed that internal neutrons made a very low to negligible contribution to neutron dose equivalent, largely attributed to the measurement location being perpendicular to the primary proton beam. The energy distributions for each of the fluence spectra (Fig. 1) were similar, with a high-energy direct neutron peak, an evaporation peak, a thermal peak, and an intermediate continuum between the evaporation and thermal peaks. Comparing Figures 1 and 2, it is clear that neutrons in the evaporation peak made the largest contribution to the dose equivalent. This is because of both their relative abundance and their high-quality conversion coefficients, the highest over this energy range (32, 33). Neutron fluence and ambient dose equivalent were approximately 1.6 times higher for the brain field than for the spine fields (Figs. 1 and 2). This is attributed to the higher range and modulation for the brain field than for the spine fields (Table 2). For the whole brain and upper spine fields, there was a nearly negligible difference in the fluence for the different phantom scenarios (Figs. 1b, d and 2b, d); differences between no phantom at isocenter and either a water or anthropomorphic phantom were <2%. This indicates that at 50 cm from isocenter for these fields, there was essentially no contribution from internal neutrons. At this large distance, neutrons created within the patient volume irradiated by the fields would have been attenuated by the intermediating tissue. A limitation of our

Table 3 Neutron dose equivalents (mSv) for a 23.4-Gy course of craniospinal irradiation for whole-brain, upper spine, and lower spine fields at 50 cm and 30 cm from isocenter as a function of depth in water

	Dose equivalent (mSv) for proton dose 23.4 Gy to beam isocenters					
	50 cm from isocenter			30 cm from isocenter		
Depth (cm)	Whole brain	Upper spine	Lower spine	Whole brain	Upper spine	Lower spine
0.1	92.2	65.3	63.4	133.2	94.3	91.6
1	92.0	65.1	63.3	133.1	94.2	91.5
2	91.7	65.0	63.1	132.5	93.8	91.2
3	87.9	62.2	60.4	127.1	90.0	87.4
5	83.3	59.0	57.3	121.6	86.1	83.7
6	79.7	56.5	54.8	116.8	82.7	80.3
8	74.1	52.5	51.0	110.1	78.0	75.7
10	66.1	46.8	45.4	98.9	70.0	68.0
12	58.8	41.7	40.5	88.3	62.6	60.8
14	54.0	38.2	37.2	82.8	58.7	57.0
16	45.4	32.1	31.2	70.4	49.9	48.4
18	39.0	27.6	26.8	59.7	42.3	41.1
19.9	31.9	22.6	21.9	50.0	35.4	34.4

study is that measurements were only performed perpendicular to the beam axis and not at varying angles to the axis of the beam.

These results are consistent with data from prostate fields reported for the Hitachi beam line by Fontenot et al (18) indicating that neutron dose to organs beyond 50 cm from proton beam isocenter was entirely due to external neutrons. For the upper spine, some minor differences were observed between the different phantom scenarios. Specifically, the total fluence was approximately 16% higher when measurements were made with water phantom at isocenter compared with measurements with no phantom at isocenter. This difference in fluence translated to a difference of 20% in the ambient dose equivalent. This suggests that, beyond 50 cm from the upper spine field, although external neutrons were the dominant component of the neutron dose, there was also some small contribution from internal neutrons. We speculate that this was observed only for this field and not the others because the upper spine field (defined by the aperture opening) was longer than the lower spine field, and thus the distance from the edge of this field was closer to the measurement location. These findings are not inconsistent with the literature. Fontenot et al (18) reported that approximately 15% of the neutron dose was attributed to internal neutrons at 30 cm from isocenter. Although the distance in that study was closer than that used in our study, that study considered only small prostate fields, whereas we considered a large spine field.

Most of the Monte Carlo literature (21, 38) reports organ dose equivalents or total effective dose equivalents for the entire treatment, meaning the sum from all CSI fields. In our study it was not possible to sum the dose equivalents from the 3 fields, because although all of our measurements were at 50 cm from isocenter, this point is at a different location in the body for each field. Studies by Newhauser et al (22) and Taddei et al (39) reported neutron dose equivalents for individual fields in a CSI treatment for the Hitachi beam line. However, those dose equivalents were reported for various organs and structures rather than at specified distances from isocenter, as in our work. To compare our results with data from those 2 studies, we had to determine which of the organs from the previous studies were at distances out-of-field comparable to those for the data reported here. We were able to review the CT scan of the patient that was used in the study by Taddei et al (39), allowing us to select organs whose positions were between 30 cm and 50 cm from the isocenter of each field and to compare data from our study and their study (Table 4).

Overall, our data are in reasonable agreement with those of Taddei et al (39), with some differences; generally, the dose equivalents in our study were somewhat higher. The differences can in part be attributed to our reporting point doses, whereas Taddei et al reported mean dose to organs that spanned a range of depths. The differences in dose equivalents between the 2 studies can also be attributed to numerous other factors, including comparison of point doses to dose averages calculated over the entire organ and our application of a depth−dose correction rather than the more detailed particle tracking used by Taddei et al (39). However, it should not be overlooked that there are differences between the Hitachi and Mevion beamline designs that directly affect the neutron production and neutron doses for proton CSI from these 2 studies. Given all of these factors, the dose equivalents reported in this study are in good agreement with those of Taddei et al (39). As previously mentioned, we cannot compare our data with most of what is in the literature, where neutron doses for CSI were not reported on an individual field basis or were reported as effective doses to the entire body, or position of the organ was not specified (relative to isocenter). However, our data agree well with those of Taddei et al (39), which were in reasonable agreement with the data from these other studies (21, 22, 38).

We can also compare our data with out-of-field stray dose (due to scatter and leakage radiation) from photon CSI. Using the analytical model reported by Taddei et al (40) for out-of-field stray dose from 6-MV photon CSI, we estimated that at 50 cm from the isocenter, photon CSI would result in 1.10 × 10-03 mSv/Gy and 5.00 × 10-02 mSv/Gy for Varian 2100 and Siemens Artise linacs, respectively. These photon doses are orders of magnitude lower than the secondary neutron doses for the various CSI proton fields reported here, 2.27 to 3.95 mSv/Gy at 50 cm from the isocenter (Table 2). However, this type of comparison can be misleading because in actuality it has been shown in the literature (21) that dose to nontarget organs is far greater for photon CSI than for proton CSI, and in

Table 4 Comparison of dose equivalents per proton Gy to isocenter from Taddei et al (39) and this study

	Range (low and high values) of neutron dose equivalents per proton Gy delivered to isocenter for CSI fields (mSv/Gy)					
	Whole brain		Upper spine		Lower spine	
Study	Low value	High value	Low value	High value	Low value	High value
Taddei et al	0.9	4.5	1.0	2.7	0.9	2.4
This study	1.4	5.7	1.0	4.0	0.9	3.9

Here, we specifically report the range of dose equivalents from Taddei et al (39) for organs whose locations were between 30 and 50 cm from the respective beam isocenters. Those values were compared with the ranges of doses listed in Table 3 for each field (note that data from Table 3 were normalized per proton Gy in Table 4).

particular for organs anterior to the spinal canal. This difference is driven by the high exit dose from photon therapy; the total photon organ dose is the sum of the exit dose and the out-of-field stray dose, whereas for protons, there is almost no exit dose and the organ dose is almost entirely due to neutrons.

In this study we report neutron doses but have not specifically addressed the risk of second cancers in children and adolescents who receive passively scattered proton therapy with the Mevion single-room, passively scattered proton system. Because these were point measurements and not organ-specific doses, it is difficult to calculate risk of second cancers to specific organs. However, because the neutron doses reported here are consistent and in relatively good agreement with organ doses from detailed Monte Carlo studies that were used to predict second cancer risk (21, 22, 38, 39), it is reasonable to hypothesize that the risk of second cancers from proton CSI delivered on the Mevion single-room, passively scattered proton system is similar to that from other passively scattered proton systems (ie, the Hitachi beam line). Nonetheless, efforts should be made to further reduce secondary neutron dose in proton therapy. To reduce the neutron dose, brain fields can be strategically designed to introduce as little brass as possible. The advent of beam scanning will also reduce neutron exposure as the brass component, along with other field-shaping apparatus, are removed.

Conclusion

In this study we measured neutron spectra and characterized neutron dose equivalents for a clinical treatment for a single gantry proton system, whose use and planned installations in the United States have recently increased. Importantly, we considered CSI, commonly used proton therapy for pediatric cancer, and found that the neutron dose from this gantry system is, overall, consistent with dose equivalents reported for CSI carried out with other proton therapy beamlines.

References

1. Hansen EK, Roach M. Handbook of Evidence-Based Radiation Oncology. New York: Springer; 2010.
2. Woo SY. Rationale for proton therapy in pediatric malignancies. In: Linz U, editor. *Ion Beam Therapy*, Vol. 320. New York: Springer-Verlag; 2012. p. 277-286.
3. Yock TI, DeLaney TF, Esty B, et al. Pediatric Tumors. Philadelphia, PA: Lippincott Williams and Wilkins; 2008.
4. Lee CT, Bilton SD, Famiglietti RM, et al. Treatment planning with protons for pediatric retinoblastoma, medulloblastoma, and pelvic sarcoma: How do protons compare with other conformal techniques? *Int J Radiat Oncol Biol Phys* 2005;63:362-372.
5. Miralbell R, Lomax A, Bortfeld T, et al. Potential role of proton therapy in the treatment of pediatric medulloblastoma primitive neuroectodermal tumors: Reduction of the supratentorial target volume. *Int J Radiat Oncol Biol* 1997;38:477-484.
6. Slater JD, Yuh GE, Loredo LN, et al. Reducing toxicity from craniospinal irradiation: Using proton beams to treat medulloblastoma in young children. *Cancer J* 2004;10:386-390.
7. St Clair WH, Adams JA, Bues M, et al. Advantage of protons compared to conventional x-ray or IMRT in the treatment of a pediatric patient with medulloblastoma. *Int J Radiat Oncol Biol Phys* 2004;58:727-734.
8. Athar BS, Paganetti H. Neutron equivalent doses and associated lifetime cancer incidence risks for head and neck and spinal proton therapy. *Phys Med Biol* 2009;54:4907-4926.
9. Howell RM, Giebeler A, Koontz-Raisig W, et al. Comparison of therapeutic dosimetric data from passively scattered proton and photon craniospinal irradiations for medulloblastoma. *Radiat Oncol* 2012;7:116.
10. Gottschalk B. Neutron dose in scattered and scanned proton beams: In regard to Eric J. Hall (*Int J Radiat Oncol Biol Phys* 2006;65:1-7). *Int J Radiat Oncol Biol Phys* 2006;66:1594. author reply 1595.
11. Paganetti H, Bortfeld T, Delaney TF. Neutron dose in proton radiation therapy: In regard to Eric J. Hall (*Int J Radiat Oncol Biol Phys* 2006; 65:1-7). *Int J Radiat Oncol Biol Phys* 2006;66:1594-1595. author reply 1595.
12. Dhall G. Medulloblastoma. *J Child Neurol* 2009;24:1418-1430.
13. Gajjar A, Chintagumpala M, Ashley D, et al. Risk-adapted craniospinal radiotherapy followed by high-dose chemotherapy and stem-cell rescue in children with newly diagnosed medulloblastoma (St Jude Medulloblastoma-96): Long-term results from a prospective, multicentre trial. *Lancet Oncol* 2006;7:813-820.
14. Gilbertson RJ. Medulloblastoma: Signalling a change in treatment. *Lancet Oncol* 2004;5:209-218.
15. Inskip PD, Curtis RE. New malignancies following childhood cancer in the United States, 1973-2002. *Int J Cancer* 2007;121:2233-2240.
16. Ning MS, Perkins SM, Dewees T, et al. Evidence of high mortality in long term survivors of childhood medulloblastoma. *J Neurooncol* 2015;122:321-327.
17. Zheng Y, Newhauser W, Fontenot J, et al. Monte Carlo study of neutron dose equivalent during passive scattering proton therapy. *Phys Med Biol* 2007;52:4481-4496.
18. Fontenot J, Taddei P, Zheng Y, et al. Equivalent dose and effective dose from stray radiation during passively scattered proton radiotherapy for prostate cancer. *Phys Med Biol* 2008;53:1677-1688.
19. Zacharatou Jarlskog C, Paganetti H. Risk of developing second cancer from neutron dose in proton therapy as function of field characteristics, organ, and patient age. *Int J Radiat Oncol Biol Phys* 2008;72:228-235.
20. Taddei PJ, Mahajan A, Mirkovic D, et al. Predicted risks of second malignant neoplasm incidence and mortality due to secondary neutrons in a girl and boy receiving proton craniospinal irradiation. *Phys Med Biol* 2010;55:7067-7080.
21. Zhang R, Howell RM, Taddei PJ, et al. A comparative study on the risks of radiogenic second cancers and cardiac mortality in a set of pediatric medulloblastoma patients treated with photon or proton craniospinal irradiation. *Radiother Oncol* 2014;113:84-88.
22. Newhauser WD, Fontenot JD, Mahajan A, et al. The risk of developing a second cancer after receiving craniospinal proton irradiation. *Phys Med Biol* 2009;54:2277-2291.
23. Clasie B, Wroe A, Kooy H, et al. Assessment of out-of-field absorbed dose and equivalent dose in proton fields. *Med Phys* 2010;37:311-321.
24. Farah J, Mares V, Romero-Exposito M, et al. Measurement of stray radiation within a scanning proton therapy facility: EURADOS WG9 intercomparison exercise of active dosimetry systems. *Med Phys* 2015; 42:2572-2584.
25. Howell RM, Burgett EA. Secondary neutron spectrum from 250-MeV passively scattered proton therapy: Measurement with an extended-range Bonner sphere system. *Med Phys* 2014;41:092104.
26. Mevion Medical Systems. Mevion S250 locations. Available at: http://mevion.Com/s250-map. Accessed November 12, 2015.
27. Burgett EA. A Broad Spectrum Neutron Spectrometer Utilizing a High Energy Bonner Sphere Extension. Atlanta: Georgia Institute of Technology; 2008.

28. Howell RM, Burgett E, Hertel NE, et al. Measurement of high-energy neutron spectra with a Bonner sphere extension system. *Nucl Technol* 2009;168:333-339.
29. Burgett EA, Reginatto M, Wiegel B, et al. UMGjava: A software package for unfolding and further analysis of data from particle spectrometers. *Trans Am Nucl Soc* 2010;103:627-628.
30. Reginatto M, Goldhagen P, Neumann S. Spectrum unfolding, sensitivity analysis and propagation of uncertainties with the maximum entropy deconvolution code maxed. *Nucl Instrum Methods A* 2002; 476:242-246.
31. Pelowitz DB. *MCNPX 2.6.0 manual, la-cp-07-1473*. Los Alamos National Laboratory; 2008.
32. ICRP, 1996. Conversion Coefficients for use in Radiological Protection against External Radiation. ICRP Publication 74. Ann. ICRP 26 (3-4).
33. International Commission on Radiation Units and Measurements. Conversion coefficients for use in radiological protection against external radiation. Bethesda, MD: Los Alamos National Laboratory; 1998.
34. d'Errico F, Luszik-Bhadra M, Nath R, et al. Depth dose-equivalent and effective energies of photoneutrons generated by 6-18 MV x-ray beams for radiotherapy. *Health Phys* 2001;80:4-11.
35. Howell R, Hertel N, Wang Z, et al. Secondary neutron spectra from high energy IMRT and conventional treatment plans using Bonner spheres and Au-197 activation foils. *Med Phys* 2005;32:2060.
36. Kry SF, Salehpour M, Followill DS, et al. Out-of-field photon and neutron dose equivalents from step-and-shoot intensity-modulated radiation therapy. *Int J Radiat Oncol Biol* 2005;62: 1204-1216.
37. Kry SF, Salehpour M, Followill DS, et al. The calculated risk of fatal secondary malignancies from intensity-modulated radiation therapy. *Int J Radiat Oncol Biol* 2005;62:1195-1203.
38. Zhang R, Howell RM, Giebeler A, et al. Comparison of risk of radiogenic second cancer following photon and proton craniospinal irradiation for a pediatric medulloblastoma patient. *Phys Med Biol* 2013;58:807-823.
39. Taddei PJ, Mirkovic D, Fontenot JD, et al. Stray radiation dose and second cancer risk for a pediatric patient receiving craniospinal irradiation with proton beams. *Phys Med Biol* 2009;54:2259-2275.
40. Taddei PJ, Jalbout W, Howell RM, et al. Analytical model for out-of-field dose in photon craniospinal irradiation. *Phys Med Biol* 2013;58: 7463-7479.